Range, velocity and immersion estimation of a moving target in a water-filled tank with an active sonar system

Alexis Mours, Jerome I. Mars, Cornel Ioana, Nicolas Josso, Yves Doisy, Philippe Roux

Range, velocity and immersion estimation of a moving target in a water-filled tank with an active sonar system

Alexis Mours*, Jérôme I. Mars*, Cornel Ioana*, Nicolas F. Josso†, Yves Doisy†, Philippe Roux‡
*Univ. Grenoble Alpes, GIPSA-Lab, F-38000 Grenoble France
CNRS, Gipsa-Lab, F-38000 Grenoble France
Email: alexis.mours@gipsa-lab.fr
†Thales Underwater Systems, 525 route Dolines, 06901 Sophia-Antipolis, France
Email: nicolas.josso@fr.thalesgroup.com
‡Univ. Grenoble Alpes, ISTerre, 1381 rue de la Piscine, 38400 Saint Martin d´Hères, France
Email: philippe.roux@ujf-grenoble.fr

***Abstract*—The knowledge of the impulse response of the propagation channel is required for many underwater applications as communication, sonar detection and localization, marine mammals monitoring, etc. In the context of target classification, this impulse response informs about the relative motion between the source/receiver and the target through the Doppler effect. Knowing the emitted signal, the Doppler compression coefficient of each acoustic path can be estimated with the wideband ambiguity plan [1]–[3]. Warping operator based-filter and wideband ambiguity plan can be used to separate acoustic paths in order to remove interferences and estimate properly the target distance and speed [4]. This paper presents a complementary approach to jointly estimate the distance and speed of the target at a small speed with reasonable resolutions. The investigated sources are Binary Phase Shift Keying (BPSK), 22-Welch-Costas, and Pulse Train Frequency Modulation (PTFM) signal. Sources have a large Time-Bandwidth product (high TB) and provide high resolutions. For this reason, an echo model that takes into account a signal temporal compression (Doppler effect) can be used. A reduced-scale laboratory experiment was conducted to estimate the speed vector and depth of a moving target. Results for speed vectors are compared for the three different sources. A ray back propagation algorithm was used and results show correct estimation of the target depth.**

I. Introduction

Active sonar systems are often used to jointly estimate the position and the velocity of a moving target. In an ocean waveguide and a deep water context, the target motion adds complexity to the scattered waves. Bertsatos and Makris had shown that an instantaneous velocity of randomly moving target swarms can be estimated by a Doppler analysis [5]. Josso *et al* had shown on real active data that different Doppler scaling factors should be taken into account in order to obtain accurate impulse response estimates [4]. Another study had also shown in an active tomography context that source/receiver motion can be corrected by estimating Doppler coefficient for each acoustic path [6]. This study proves that the use of the wideband ambiguity plan is very efficient with large time-bandwidth signals for speed measurements. The proposed paper investigates a complementary approach, that estimates position and velocity of a moving target at low speed with different types of source in a reduced-scale experiment. An active sonar case study with large time-bandwidth (high TB) signals in a deep-ocean environment with an horizontal moving target are considered. In a first part, wideband Doppler model, wideband ambiguity function and conventional beamforming are presented. Then the experimental protocol and the emitted signals are described. Speed estimation results are compared for three different waveforms. The target speed vector is derived and the target immersion is finally estimated using a localization algorithm based on rays back propagation [7].

II. Wideband Doppler model

Consider a wideband complex (analytic) signal in the form of a modulated carrier,

$$s(t) = \mu(t)\, e^{2i\pi f_c t} \tag{1}$$

where $\mu(t)$ is the complex envelope, and f_c is the carrier frequency. Analytic signals can be found by using Hilbert transform. Assume that the real emitted signal is reflected by a moving target, which can be modeled as a point. Due to a relative motion between the source/receiver (mono-static sonar) and the target, echoes will be modified by the Doppler effect. The signal received by a transducer for a single acoustic path can be written in the form

$$x(t) = \sqrt{\eta_0}\, s[\eta_0(t-\tau_0)] \tag{2}$$

where η_0 is the target Doppler compression coefficient and τ_0 is the target round-trip delay related to a single acoustic path. The factor $\sqrt{\eta_0}$ is used to conserve the signal energy. Using (1), (2) becomes

$$x(t) = \underbrace{\sqrt{\eta_0}\, \mu[\eta_0(t-\tau_0)]}_{\text{First effect}}\ \underbrace{e^{2i\pi f_c \eta_0 (t-\tau_0)}}_{\text{Second effect}} \tag{3}$$

Relative velocity between target and source has two effects on signal. The first is a compression or dilatation of the time scale of the complex envelope together with an amplitude change. The second is a carrier frequency shift. When dealing with large time-bandwidth signals, or mathematically when

$$\frac{TB^2}{f_c} \gg 1 \tag{4}$$

978-1-4799-8736-8/15/$31.00 ©2015 IEEE

where T is the signal duration and B is the signal spectral bandwidth, the received signal model has then to take into account the two effects [2]. If the signal is narrow band, then the former can be neglected and the received signal becomes

$$x(t) = \mu(t - \tau_0)\, e^{2i\pi f_c \eta_0 (t-\tau_0)} \tag{5}$$

III. Wideband ambiguity function

The wideband Doppler model shows that a punctual target can be defined by two parameters : the target round-trip delay τ_0 and the relative target Doppler compression coefficient η_0. These parameters can be estimated by cross correlating the received signal $x(t)$ against a set of reference signals. Each reference signal $r_\eta^\dagger$ is a time-compressed or time-expanded version of the original transmitted signal :

$$r_\eta^\dagger(t) = \sqrt{\eta}\, s(\eta t) \tag{6}$$

A cross-correlation $R(\tau, \eta)$ is computed for each combination of delay τ and η to cover the full range of expected target delay and relative Doppler compression coefficient :

$$R(\tau, \eta) = \int_{-\infty}^{+\infty} r_\eta^\dagger(t - \tau) x(t)\, dt \tag{7}$$

where $\dagger$ denotes complex conjugation and $x(t)$ is the analytic representation of the real received signal. Using equations (2) and (6), it can be re-written as

$$R(\tau, \eta) = \sqrt{\eta\eta_0} \int_{-\infty}^{+\infty} s[\eta(t - \tau)] s[\eta_0(t - \tau_0)]\, dt \tag{8}$$

Then by introducing the substitution $t' = t - \tau$, equation (8) becomes

$$R(\tau, \eta) = \sqrt{\eta\eta_0} \int_{-\infty}^{+\infty} s(\eta t) s[\eta_0(t - \tau_0 + \tau)]\, dt \tag{9}$$

The wideband ambiguity function (WAF) introduced by J.P. Hermand, [3] is written as

$$\chi(\tau, \eta) = \left| \frac{R(\tau, \eta)}{R(0, 1)} \right| \tag{10}$$

where $R(0, 1) = \int_{-\infty}^{+\infty} |s(t)|^2\, dt$ is the original signal energy. When $\tau = 0$ and $\eta = 1$, the received and transmitted signal are identical and the function is called the wideband autoambiguity function. It describes the accuracy, ambiguity and resolution properties of a waveform. When the received signal is modified by the propagation channel, the function used to estimate the target delay and Doppler coefficient is called the (wideband) delay-doppler plan or delay-speed plan, depending on chosen axes. Figures presented in this studies will always represent the squared magnitude of these functions. Assuming that noise is additive, white and gaussian, maximum likelihood (ML) estimation is used to estimate the target parameters (τ_0, η_0).

$$(\hat{\tau_0}, \hat{\eta_0}) = \arg\max_{(\tau,\eta)} \left\{ |\, R(\tau, \eta)\, |^2 \right\} \tag{11}$$

The delay estimate $\hat{\tau_0}$ and the doppler coefficient estimate $\hat{\eta_0}$ are the parameters which maximizes the squared magnitude of the delay-doppler plan and provides the range and the speed of the target.

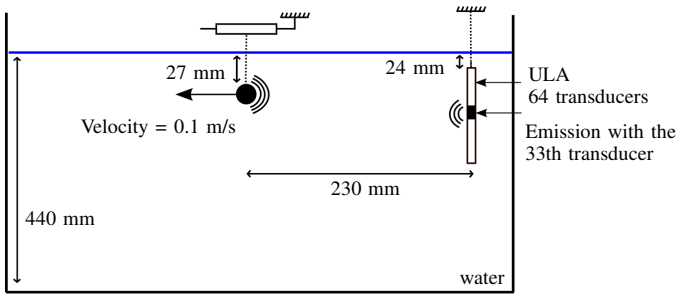

Fig. 1. Water-filled tank experimental set-up. The experiment is composed of a vertical antenna and a moving spherical target. A waveform is emitted by the 33^{th} transducer when the target has reached the constant speed $V = 0.1 m.s^{-1}$.

IV. Conventional beamforming

In the general case, echoes travel through multiple acoustic paths. So the received signal is a combination of echoes with different amplitudes, Doppler coefficients and delays :

$$y_n(t) = \sum_{i=1}^{M} a_i\, x_i(\eta_i(t - \tau_i)) \tag{12}$$

where $y_n(t)$ is the received signal for the transducer n, M is the number of acoustic path, $x_i(t)$, a_i, η_i and τ_i are respectively the signal, the amplitude, the Doppler coefficient and the delay related to the i^{th} acoustic path. When multiple transducers are available to record acoustic waves, it is possible to dispose them in a linear uniform antenna, where the distance between two successive transducers (d) is equal to an half-wavelength. Such antennas are used to perform beamforming, which is a signal processing technique used for directional signal transmission or reception [8]. Therefore, a signal coming from the elevation angle ϕ can be written as

$$y_\phi(t) = \frac{1}{N} \sum_{n=1}^{N} y_n(t + \tau_n) \tag{13}$$

where N is the number of transducers in the array and τ_n is the delay related to the n^{th} transducer :

$$\tau_n(\phi) = \frac{ndsin\phi}{c} \tag{14}$$

where ϕ is the angle between the wave arrival direction and the orthogonal direction to the antenna. The antenna angular resolution, called the half power beam width [9], may be approached by :

$$2\phi_{3dB} = \frac{50\lambda}{Nd}\ \text{deg} \tag{15}$$

V. Laboratory experiment

The wideband ambiguity plan improves the joint estimation of target delay and Doppler coefficient for each acoustic path when (4) is met. We propose an active sonar scenario in a shallow water environment that was reproduced in the water experimental tank of IsTerre laboratory [10]. Dimensions of the water tank are 1.9 m x 0.9 m x 0.6 m. A scaling factor of 200:1 is used to model a 5 kHz active source in a deep ocean with a 0.7 m-diameter spherical target at a speed of

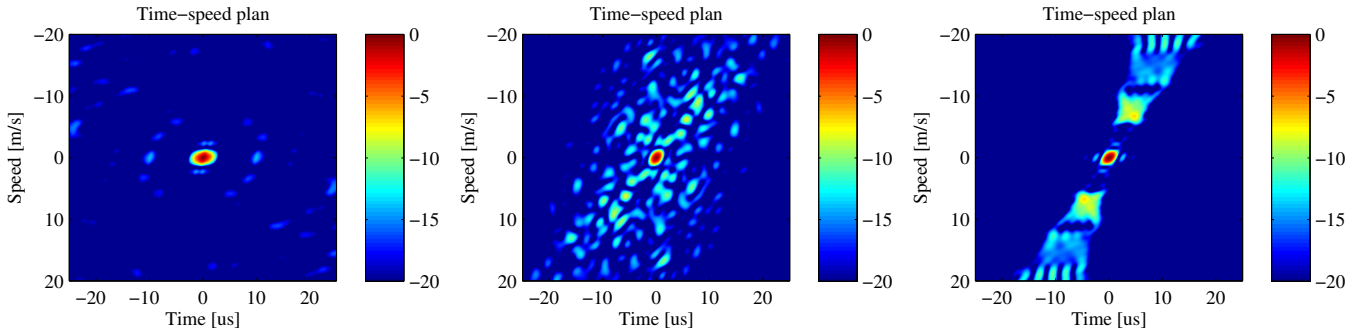

(a) BPSK (b) 22-Welch-Costas (c) PTFM, $N = 5$

Fig. 2. Wideband ambiguity functions of BPSK signal (2a), 22-Welch-Costas signal (2b), and PTFM signal (N = 5) (2c). T =500 μs et B = 600 kHz.

0.1 $m.s^{-1}$. At the real scale, the metallic target is immersed at 5.4 m and the first hydrophone of the vertical uniform linear array (ULA) is at a depth of 4.8 m. The ULA is 112 m away from the target when the waveform is emitted. At the laboratory scale, the ULA is composed of half-wavelength spaced 64 transducers that have a 1 MHz carrier frequency and a 1 MHz bandwidth at -6 dB with a sampling frequency of $F_e = 20MHz$. The target is a 3.5 mm spherical lead used for fishing hanged from a motorized arm. The experimental set up is described in Fig.1. The motorized arm is used to set in position the target accurately and move it horizontally. The target is 230 mm away from the transducer array at the time $t = 0$ and they are both close enough to the air-water interface to ensure that the bottom-reflected path is not present. The target is then shifted 550 mm to the left at a horizontal constant velocity of 0.1 $m.s^{-1}$, as shown on the Fig.1. Emission of the waveform is realized with the transducer, that is in the middle of the ULA, to create a spherical wave that propagates in all elevation angles with a small azimuth beam width. This experiment focus on estimating the target position and speed with only one waveform.

A. Emitted waveforms

Waveforms have a 600 kHz bandwidth and a 500 μs duration, and thus a time-bandwidth product of 300, which justify the use of the wideband Doppler model. It would be more difficult to emit a longer signal, because echoes back-scattered from the tank background will be scrambled with signals of interest. The wideband ambiguity function is used to describe the time and speed resolutions at -3 dB for the synthetic waveforms. Resolutions are computed by taking coordinates of the major axis of the -3 dB main lobe edge.

1) Binary phase shift keying (BPSK) signal: Let $s(t)$ be a binary phase modulated signal of the form,

$$s(t) = e^{i\pi c(t)}\, e^{2i\pi f_p t} \tag{16}$$

where $c(t)$ is a binary sequence, which contains N symbols. The symbol duration θ was fixed by the spectral bandwidth B, $\theta = 2/B$. Then, the binary sequence duration is $N\theta$.

2) Costas signal: Costas waveforms are frequency hopped pulse trains. The waveform is divided in N subpulses of equal duration. Each subpulse transmit a unique frequency chosen from a set of N available frequencies [11]. These are described by a Costas sequence θ_n, which can be generated by the Welch-Costas method [12] [13]. This method takes a primitive number g of a prime number N and generates a sequence from the $N = p-1$ successive powers of g modulo p. In this paper, the Welch-Costas sequence θ_n with $N = 23$ and $g = 5$ is used : $\{5,2,10,4,20,8,17,16,11,9,22,18,21,13,19,3,15,6,7,12,14,1\}$. The subpulse frequency is given by

$$f_n = (f_c - \frac{B}{2}) + (\theta_n - 1)\frac{B}{N-1} \quad \text{for } 0 \le n \le N-1 \tag{17}$$

The analytic form of Welch-Costas signal is

$$s(t) = \sum_{n=0}^{N-1} p_n(t - nT_s) \tag{18}$$

where $p_n(t) = \begin{cases} e^{2i\pi f_n t} & \text{for } 0 \le t \le T_s \\ 0 & \text{elsewhere} \end{cases}$ and T_s is the subpulse duration.

3) Pulse train frequency modulation (PTFM) signal: PTFM is a pulse train of linear frequency modulation (LFM). The waveform is divided in N subpulses of equal duration. Each subpulse transmit a LFM. The analytic form of a PTFM signal is the same as Welch-Costas signal (18), where

$$p_n(t) = \begin{cases} e^{2i\pi(f_c + \frac{B}{2T}t)t} & \text{for } 0 \le t \le T_s \\ 0 & \text{elsewhere} \end{cases} \tag{19}$$

and T_s is the subpulse duration.

Fig.2 presents the wideband ambiguity functions of the BPSK signal (Fig.2a), 22-Welch-Costas signal (Fig.2b) and the PTFM signal (with N=5) (Fig.2c). These WAF show main lobes centered in ($\tau = 0, V = 0$). 22-Welch-Costas WAF shows higher side lobes than BPSK WAF. PTFM shows higher and more localized side lobes than others. Moreover, the pattern on the PTFM WAF, shown in Fig.2c, is repeated at multiples $\pm T_s$ and $\pm 2T_s$ with a decreasing magnitude. BPSK signal seems to have good properties compared to others. Time and speed resolution of each synthetic waveform are resumed in the Table I. The three waveforms have close time and speed resolutions. BPSK and 22-Welch-Costas signals will be less sensitive to interferences compared to PTFM, because the energy of side lobes is more spread out over the delay-Doppler plan. The difference of arrival times between two successive

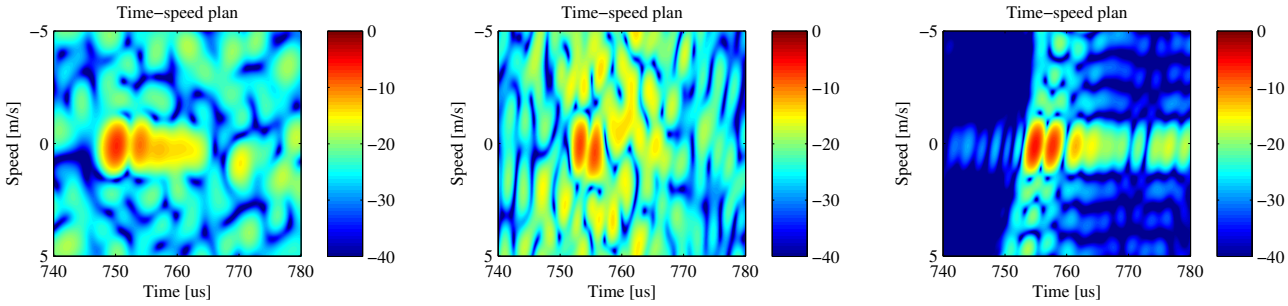

(a) Direct path, BPSK (b) Direct path, 22-Welch-Costas (c) Direct path, PTFM, $N = 3$

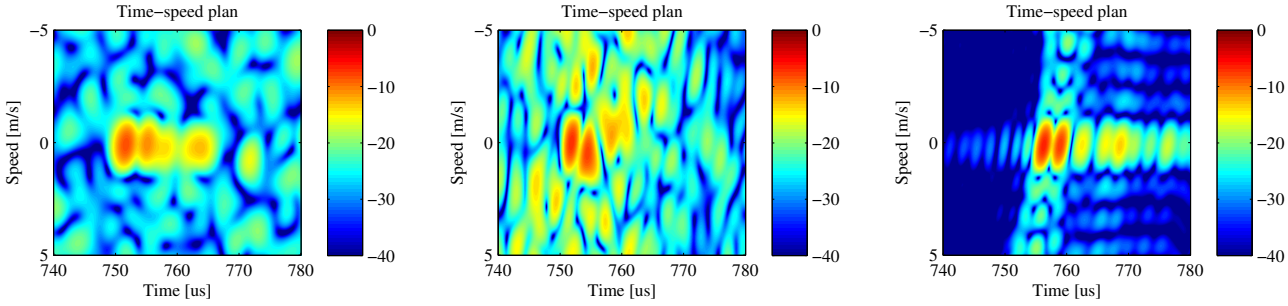

(d) Surface-reflected path, BPSK (e) Surface-reflected path, 22-Welch-Costas (f) Surface-reflected path, PTFM, $N = 3$

Fig. 3. Wideband ambiguity plans, for direct path (Elevation angle $\phi_d = 2.92$ deg) and surface-reflected path (Elevation angle $\phi_s = 8.23$ deg), of BPSK signal (3a), 22-Welch-Costas signal (3b), and PTFM signal (N = 3) (3c). T = 500 μs and B = 600 kHz.

TABLE I. TIME (OR DISTANCE) AND SPEED RESOLUTION AT -3dB FOR THE THREE WAVEFORMS.

	Time resolution or distance resolution	Speed resolution
BPSK	1.03 μs / 1.53 mm	0.69 $m.s^{-1}$
22-Welch-Costas	0.93 μs / 1.39 mm	0.69 $m.s^{-1}$
PTFM	0.88 μs / 1.32 mm	0.67 $m.s^{-1}$

echoes of the same acoustic path should be higher than the time resolution in order to separate them in time.

VI. EXPERIMENTAL RESULTS

In this section is explained the experimental results for the speed estimation of a slow-moving target. The goal of this experimental part is to estimate the target speed during its motion with only one waveform emission. Each waveform is emitted at the fixed time $t = 4.5\,s$ after the start of the target so that the speed is constant. The conventional beamforming is used on received signals to detect the most energetic paths, which are the direct and the surface-reflected path. The detection curve for the three sources is shown on the Fig.4. The elevation angle is $\phi_d = 2.9\,\text{deg}$ for the direct path and $\phi_s = 8.2\,\text{deg}$ for the surface-reflected path. Angles are defined positives when they points upwards. The wideband ambiguity plan can then be applied to the two beamformed signals. The pixel size of the wideband ambiguity plan is $\Delta\tau = 1/Fe$ and $\Delta V = 0.01\,m.s^{-1}$ ($V_{3dB}/70$). So the estimation error at this step will be small compared to the expected and estimated values.

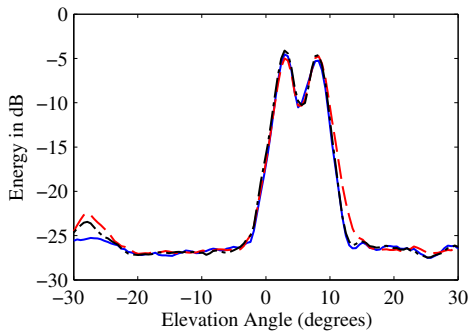

Fig. 4. Elevation estimation for the two acoustic path.BPSK (Blue). 22-Welch-Costas (Red color, –). PTFM (Black color. -.). $\phi_{direct} = 2.92\,\text{deg}$, $\phi_{surface} = 8.23\,\text{deg}$.

Fig.3 presents the wideband ambiguity plans for the three sources (columns) and for the direct and surface-reflected path (rows). The interval of the speed axis is $[-5\,m.s^{-1}, +5\,m.s^{-1}]$, because values out of this limits do not correspond to the expected speed. Fig.3 shows that the time of arrival of echoes are different of a few microseconds for the three waveforms, and it may be a synchronization problem. It can be noticed that two echoes are present in each figure. The first echo is a direct reflection of the wave from the target, while the second echo is probably an elastic wave passing through the target or a surface wave (Rayleigh wave). Echoes are well resolved in time, so the delay and speed estimation of the first echo is not biased. Delay-speed plans are coherent with those expected in the case of two bright spots. Estimations of the target speed and delay are resumed in the Tab.II.

TABLE II. ESTIMATION OF THE RELATIVE RADIAL SPEED $[m.s^{-1}]$ AND DELAYS $[\mu s]$, FOR DIRECT ($\phi_d = 2.9$ deg) AND SURFACE-REFLECTED ($\phi_s = 8.2$ deg) ACOUSTIC PATH, FOR THE THREE WAVEFORM. IN THE FIRST COLUMN ARE PRESENTED RESULTS FOR THE FIRST ECHO, AND IN THE SECOND COLUMN ARE PRESENTED RESULTS FOR THE SECOND ECHO.

	First echo		Second echo	
Path	Direct	Surface	Direct	Surface
BPSK	0.09 $m.s^{-1}$ 750.2 μs	0.04 $m.s^{-1}$ 751.7 μs	0.07 $m.s^{-1}$ 754 μs	0.04 $m.s^{-1}$ 755.15 μs
Costas	-0.01 $m.s^{-1}$ 751.85 μs	0.45 $m.s^{-1}$ 753.25 μs	0.03 $m.s^{-1}$ 754.45 μs	0.39 $m.s^{-1}$ 755.6 μs
PTFM N=5	0.1 $m.s^{-1}$ 754.8 μs	0.1 $m.s^{-1}$ 756.25 μs	0.11 $m.s^{-1}$ 757.65 μs	0.09 $m.s^{-1}$ 758.9 μs

The real speed of the target is about 0.1 $m.s^{-1}$ in the horizontal direction. Direct path speed estimation are good and coherent excepted for the 22-Welch-Costas signal which has low values. Surface-reflected path speed estimation results are more mitigated. The PTFM signal shows a correct estimation of the speed and the BPSK shows a value close to the true speed. But the 22-Welch-Costas shows a high speed value that stays within the interval given by the -3dB speed resolution, so the estimated value is not incoherent.

Fig.5 presents the estimation of the target speed vector for the first bright spot (column one) and the second bright spot (column two). Each line corresponds to a waveform (BPSK, 22-Welch-Costas, PTFM). The speed vector is computed in Cartesian coordinate with a positive X-axis pointing to the left and a positive Z-axis pointing downwards.

$$\hat{v_x} = \frac{1}{2}[\hat{V_d}\cos -\hat{\phi_d} + \hat{V_s}\cos\hat{\phi_s}] \tag{20}$$

$$\hat{v_z} = \frac{1}{2}[\hat{V_d}\sin -\hat{\phi_d} + \hat{V_s}\sin\widehat{\phi_s}] \tag{21}$$

where $\hat{V} = \hat{v_x}.\overrightarrow{u_x} + \hat{v_z}.\overrightarrow{u_z}$ is the estimated speed vector of the target, $\hat{V_d}$ and $\hat{V_s}$ are the estimated speed for the direct and surface-reflected path, and $\hat{\phi_d}$ and $\hat{\phi_s}$ are the estimated angles for the direct and surface-reflected path.

In conclusion, the PTFM source with N=5 has the best results among the three. It seems that phase (BPSK) and frequency (Welch-Costas) coded waveforms are less efficient in the target speed estimation.

VII. LOCALIZATION

The next part of this article is the localization in depth of the target. The target depth is estimated by means of ray back-propagation. This method has been demonstrated for low-frequency passive sonar systems [14] and for mid-frequency active sonar system [7]. It consists of propagating rays from the antenna in the estimated elevation angles and limiting the travel time to the estimated one-way delays. The method developed in this article is mainly based on [7]. This provides a probability density function (pdf) of the target localization as a function of range and depth. Assuming a Gaussian distribution for the arrival angles and delays, the pdf of ϕ and τ are given

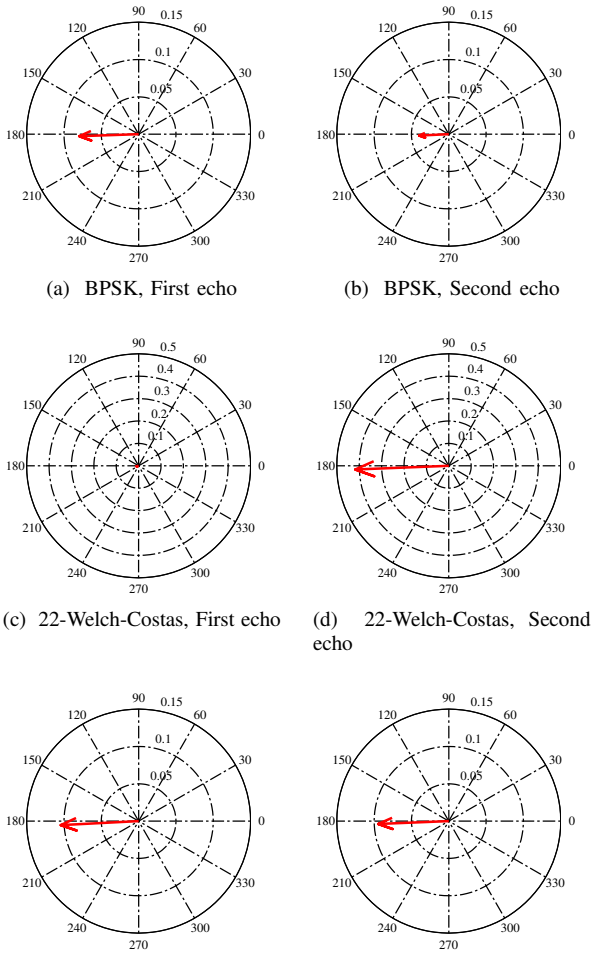

(a) BPSK, First echo (b) BPSK, Second echo

(c) 22-Welch-Costas, First echo (d) 22-Welch-Costas, Second echo

(e) PTFM, First echo (f) PTFM, Second echo

Fig. 5. Polar plot of the estimated target speed vector for the first echo (column one) and the second echo (column two). Each line corresponds to a waveform (BPSK, 22-Welch-Costas, PTFM).

by :

$$f(\phi|\hat{\phi}_i, \phi_{3dB}) = \frac{1}{\sqrt{2\pi}\phi_{3dB}}\exp\left(-\frac{(\phi-\hat{\phi}_i)^2}{2{\phi_{3dB}}^2}\right) \tag{22}$$

where $2\phi_{3dB} = 1.56$ deg is given by Eq.(15), and $\hat{\phi}_i$ is the elevation angle estimated in the previous part for the path i (direct path, surface-reflected path).

and,

$$f(\tau|\hat{\tau}_i, \tau_{3dB}) = \frac{1}{\sqrt{2\pi}\tau_{3dB}}\exp\left(-\frac{(\tau-\hat{\tau}_i)^2}{2{\tau_{3dB}}^2}\right) \tag{23}$$

where $\tau_{3dB} \simeq 1\,\mu$s is given by Tab.I and $\hat{\tau}_i$ is the one-way delay for the path i which can be approximated by the half of delay values in the Tab.II. In this section, only the first bright spot is considered.

A ray tracer program (Bellhop) with a constant sound speed profile was used to compute the times of arrival and elevation angles of rays for multiple positions of the receiver (target in this case) [15], [16]. By back-propagating the rays of the direct and surface-reflected path, a pdf of the target position

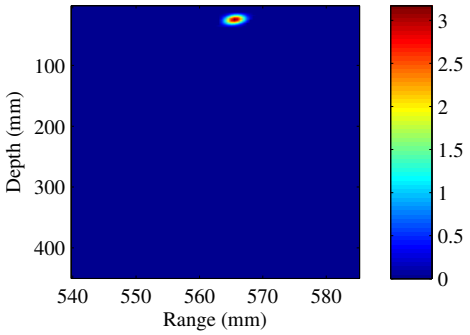

Fig. 6. Pdf of the target position in function of (r,z). The estimated target position is ($\hat{z}_t = 25.5\,mm$, $\hat{r}_t = 565.5\,mm$), the estimated resolution at -3dB is ($\hat{z}_{3dB} = 6.25\,mm$, $\hat{r}_{3dB} = 1.25\,mm$). The sampling of this grid is $\Delta z = 0.5\,mm$ by $\Delta r = 0.5\,mm$, and the number of rays emitted for a single acoustic path is N = 31, so $\Delta\phi = 0.1042$ deg.

can be performed in function of the range *r* and the depth *z*. Considering an acoustic path *i*, the probability that the target is at the position (*r,z*), $p^i_{(r,z)}$, is the product of the probability that the ray is coming from the elevation angle ϕ, p^i_ϕ, and the probability that the ray delay is τ, p^i_τ, under the assumption that the two events are independent :

$$p^i_{(r,z)} = p^i_\phi \times p^i_\tau \approx f(\phi|\hat{\phi}_i, \phi_{3dB}).\Delta\phi \times f(\tau|\hat{\tau}_i, \tau_{3dB}).\Delta\tau \tag{24}$$

where $\Delta\phi$ is the angular step between two successive rays emitted within the interval $[\hat{\phi}_i - 2\phi_{3dB},\ \hat{\phi}_i + 2\phi_{3dB}]$ to sample the grid of position (*r,z*), and $\Delta\tau = 1/F_s$ is the time duration between two samples. Only the rays that have a delay within the interval $[\hat{\tau}_i - 2\tau_{3dB},\ \hat{\tau}_i + 2\tau_{3dB}]$ are considered to compute the probability that the target is at the position (*r,z*). Assuming that acoustic paths features (τ, ϕ) are independent, then the final probability is :

$$p_{(r,z)} = p^d_{(r,z)} \times p^s_{(r,z)} = f(\phi|\hat{\phi}, \phi_{3dB})\Delta\phi \times f(\tau|\hat{\tau}_i, \tau_{3dB})\Delta\tau \tag{25}$$

and the pdf is,

$$f(r, z|\theta_d, \theta_s, \tau_d, \tau_s) \approx \frac{p_{(r,z)}}{\Delta z \Delta r} \tag{26}$$

where Δz and Δr are the receiver grid sampling in depth and range for the ray tracer program.

The antenna tilt of approximately 3.6 deg has been corrected before the localization algorithm. In the Fig.6 is plotted the pdf of the target position as a function of the depth z and range *r* with the delay results for the BPSK signal. The target position is estimated at $\hat{z}_t = 25.5\,mm$ and $\hat{r}_t = 565.5\,mm$. The true value of depth is $z_t = 27 \pm 2\,mm$, so the estimation is correct and the error is small. The resolutions at $-3\,dB$ for the depth and range are $\hat{z}_{3dB} = 6.25\,mm$ and $\hat{r}_{3dB} = 1.25\,mm$, which are reasonable. The large number of sensors ($N = 64$) and the signal bandwidth gives a high angular resolution ($\phi_{3dB} = 0.1042$ deg) and a good delay resolution ($\tau_{3dB} \simeq 1\,\mu s$). This leads to a very good depth estimation.

VIII. Conclusion

This paper shows with experimental results that the speed vector of a slowly moving target can be estimated with only one shoot of a wideband source. The BPSK, 22-Welch-Costas and PTFM (N=5) signals are compared in the target speed estimation, but the PTFM has been the best waveform among the three. Results for the others are coherent and within the interval given by the speed resolution, but they are not close enough to the true value. Wideband ambiguity plans and large time-bandwidth signals have allowed sufficient time and speed resolution with an adequate energetic spread of the side lobes. Using a ray back propagation method, the target depth estimation is very close to the true value. Future works will focus on studying the echoes of more complex target (submarine reduced-scale model, fishes), and the estimation of the depth and speed vector of these targets for classification purposes.

References

[1] Z.-b. Lin, "Wideband ambiguity function of broadband signals," *IEEE J. Acoust. Soc. Am.*, vol. 83, no. 6, pp. 2108–2116, 1988.

[2] A. W. Rihaczek, "Delay-doppler ambiguity function for wideband signals," *IEEE Trans. Aerosp. Electron. Syst.*, vol. AES-3, no. 4, pp. 705–711, Jul. 1967.

[3] J.-P. Hermand and W. I. Roderick, "Delay-Doppler resolution performance of large time-bandwidth-product linear FM signals in a multipath ocean environment," *IEEE J. Acoust. Soc. Am.*, vol. 84, no. 5, pp. 1709–1727, Nov. 1988.

[4] N. F. Josso, C. Ioana, J. I. Mars, C. Gervaise, and Y. Stéphan, "On the consideration of motion effects in the computation of impulse response for underwater acoustics inversion," *IEEE J. Acoust. Soc. Am.*, vol. 126, no. 4, p. 1739, 2009.

[5] I. Bertsatos and N. C. Makris, "Estimating the instantaneous velocity of randomly moving target swarms in a stratified ocean waveguide by doppler analysis," *IEEE J. Acoust. Soc. Am.*, vol. 130, no. 1, pp. 84–101, Jul. 2011.

[6] N. F. Josso, C. Ioana, J. I. Mars, and C. Gervaise, "Source motion detection, estimation, and compensation for underwater acoustics inversion by wideband ambiguity lag-doppler filtering," *IEEE J. Acoust. Soc. Am.*, vol. 128, no. 6, pp. 3416–3425, 2010.

[7] K. T. Hjelmervik, "Target depth estimation using a ray backpropagation scheme on mid-frequency active sonar data," *Proceedings of ECUA*, 2010.

[8] H. L. V. Trees, *Detection, Estimation, and Modulation Theory, Optimum Array Processing*. John Wiley & Sons, Apr. 2004.

[9] Bouvet.M, *Traitements des Signaux pour les Systmes Sonar. Collection Technique et Scientifique des Tlcommunications*. MASSON, Paris, Apr. 2004.

[10] P. Roux, I. Iturbe, B. Nicolas, J. Virieux, and J. I. Mars, "Travel-time tomography in shallow water: Experimental demonstration at an ultrasonic scale," *IEEE J. Acoust. Soc. Am.*, vol. 130, no. 3, pp. 1232–1241, 2011.

[11] J. Costas, "A study of a class of detection waveforms having nearly ideal range-doppler ambiguity properties," *Proceedings of the IEEE*, vol. 72, no. 8, pp. 996–1009, Aug. 1984.

[12] S. Maric, I. Seskar, and E. Titlebaum, "On cross-ambiguity properties of Welch-Costas arrays," *IEEE Trans. Aerosp. Electron. Syst.*, vol. 30, no. 4, pp. 1063–1071, Oct. 1994.

[13] S. Pecknold, W. Renaud, D. McGaughey, J. Theriault, and R. Marsden, "Improved Active Sonar Performance Using Costas Waveforms," *IEEE J. Ocean. Eng.*, vol. 34, no. 4, pp. 559–574, Oct. 2009.

[14] P. Voltz and I. Lu, "A time-domain backpropagating ray technique for source localization," *IEEE J. Acoust. Soc. Am.*, vol. 95, no. 2, pp. 805–812, 1994.

[15] M. B. Porter, "The bellhop manual and users guide: Preliminary draft," *Heat, Light, and Sound Research, Inc., La Jolla, CA, USA, Tech. Rep*, 2011.

[16] ——, "Bellhop gaussian beam/finite element beam code," *Available in the Acoustics Toolbox, http://oalib.hlsresearch.com/Rays*, 2015.